

Filament Bending Promotes Dynamic Stability in Unconventional Soft Active Nematics

Daniel S. Seara^{1,3}, Ian Linsmeier^{2,3}, A. Pasha Tabatabai^{2,3}, Patrick W. Oakes⁴, S.M. Ali Tabei⁵, Shiladitya Banerjee^{6*}, and Michael P. Murrell^{1,2,3*}

¹Department of Physics, Yale University, 217 Prospect Street, New Haven, Connecticut 06511, USA

²Department of Biomedical Engineering, Yale University, 55 Prospect Street, New Haven, Connecticut 06511, USA

³Systems Biology Institute, Yale University, 850 West Campus Drive, West Haven, Connecticut 06516, USA

⁴Department of Physics & Astronomy, and Department of Biology, University of Rochester, Rochester, New York 14627, USA

⁵Physics Department, University of Northern Iowa, Cedar Falls, Iowa 50614, USA

⁶Department of Physics and Astronomy, Institute for the Physics of Living Systems, University College London, Gower Street, London WC1E 6BT, UK

*=corresponding author

ABSTRACT

The actomyosin cytoskeleton is an active semi-flexible polymer network whose non-equilibrium behaviors regulate both cell elasticity and fluidity to maintain or change cell shape. Unlike the induction of contractile flows, the maintenance of dynamic stability in highly labile yet internally pre-stressed active materials remains unknown. To this end, we synthesize a biomimetic active nematic liquid crystal from long semi-flexible actin filaments driven out-of-equilibrium by myosin motor activity. We identify new actomyosin interactions that govern the dynamic architecture and mechanical response of the network to active stresses. These responses include dynamic steady states, in which myosin induces transverse plucking of actin filaments, whose curvatures show anomalous and strongly coupled fluctuations across a broad spectrum of filament bending modes. These fluctuations break detailed balance, yet promote dynamic stability in a network predisposed to instabilities. Furthermore, the actomyosin interactions that maintain dynamic stability are fundamentally distinct from those that drive contractile flows of actomyosin networks.

Key Words: Dynamic Stability, Contractile Flow, Elasticity, Active Nematics

INTRODUCTION

The description of the eukaryotic cytoskeleton as a viscoelastic active polar gel has described the mechanics and flow of actin in the lamellipodium¹, propagating waves during spreading², and fluctuations in the mitotic spindle³. Active gel theory has been used to describe the dynamics of topological defects in systems of purified rigid cytoskeletal filaments, namely microtubule polymer networks^{4,5}. In these systems, molecular motors slide rigid protein polymers

along their long axis, driving spontaneous flow and defect dynamics while retaining local liquid-crystalline order. By contrast, the accumulation of active stresses in systems of purified semi-flexible cytoskeletal filaments, such as actin, which has a persistence length three orders of magnitude smaller than that of microtubules, leads to destabilizing contractile flows⁶, amplification of contractile stresses⁷, and filament buckling⁸. As a consequence, networks of semi-flexible filaments experience large strains⁸, architectural changes⁹, and filament severing at high curvatures^{10, 11}. While the stability of cytoskeletal networks has thus far been attributed to fluidization of rigid filaments by molecular motors^{5, 12}, the role of filament elasticity in coordinating the dynamic stability of cytoskeletal assemblies remains unclear.

In this work, we establish three distinct material phases of quasi-2D biomimetic actin networks: nematically-ordered thermal (passive) networks, nematically-ordered active yet stable networks, and contractile networks. First, we quantify the steady state fluctuations and network organization of a passive quasi-2D biomimetic model of the F(filamentous)-actin cytoskeleton. In this model system, the network self-organizes into nematically ordered domains separated by topological defects with winding numbers $\pm 1/2$, characteristic of nematic liquid crystals^{13, 14}. We then create an active network by incorporating myosin motors, where myosin-generated active stresses either lead to 1) unstable contractile flow at high myosin densities or 2) a stable, yet dynamic, non-contractile network at lower myosin concentrations. By uncovering the relationship between contractile flow, network organization, and active stress, we show that dynamic stability is achieved through elastic “plucking” of F-actin transverse to its long axis, in stark contrast to the well-known mechanism of relative sliding between aligned F-actin and myosin during muscle contraction^{15, 16, 17}. We show that active stable states violate detailed balance by coupling all observed filament bending modes, and dissipating active stresses at all length scales.

Results

Semi-flexible F-actin networks exhibit local nematic ordering with frozen topological defects

F-actin can be crowded to the surface of a phospholipid bilayer due to the depletion forces induced by methylcellulose (MC)¹⁸ (Fig 1a,c; Supplementary Movie 1). In the absence of adhesion between the actin and membrane, the filaments change their spatial orientation to establish a net direction upon reaching the membrane surface. This reorganization of the network generates local domains of nematic alignment (Fig 1c-f, i), quantified by the coarse-grained nematic order parameter $\langle q \rangle = 2 \langle \cos^2 \theta - 1/2 \rangle$ (Fig 1b), that originate from and terminate in regions of disordered F-actin (Methods, Supplementary Figure 1, 2, Supplementary Note). The full nematic tensor order parameter gives the same behavior as the scalar parameter introduced above (Supplementary Note, Supplementary Figure 3). As F-actin densifies on the bilayer, the network transitions continuously from an isotropic to a nematic phase, which has been previously reported for actin filaments longer than $2 \mu\text{m}$ ¹⁹ (Supplementary Figure 2). The disordered domains that flank the nematic regions are comprised of disclination defects with topological charges $\pm 1/2$. Defects of charge $-1/2$ are formed by moderate F-actin bending in radial directions around a central void (Fig 1g,j), whereas defects of charge $+1/2$ form due to highly bent F-actin oriented along a single direction about a central core (Fig 1h,k). Coupling of F-actin to the phospholipid bilayer and concentration of depletion agent differentially modulate the accumulation of F-actin and the extent of its nematic ordering (Supplementary Figure 2).

The average F-actin length in our experiments is $\sim 10 \mu\text{m}$, comparable to their persistence length²⁰ and the size of the nematically ordered domains, but larger than the defect size, defined as the average linear dimension of a disordered region containing a topological defect. Nevertheless, the long, semi-flexible F-actin assembles into a quasi-2D nematic with the same

defects and symmetries characteristic of nematic liquid crystals made of short, rigid rods^{5, 21}. In this case, disclination defects originate from bending and entanglement of just a few actin filaments. Due to filament entanglement, we do not observe defect motion or annihilation (~1 hr), indicating an unconventional nematic material that is a viscoelastic solid with local nematic ordering.

Thus far, the dynamics of myosin-driven F-actin have largely been attributed to contractile flow of the actin network^{6, 8, 9, 10, 22, 23, 24, 25, 26}. Contractile networks do not yield $\pm 1/2$ defects observed in our network. Therefore, we next ask how the nematic order in actomyosin networks evolves in 1) passive, 2) active non-contractile, and 3) contractile networks.

Nematic order is preserved in non-contractile, active networks

We first quantify the effects that contractility has on the nematic order of our unconventional nematic material. By increasing the concentration of myosin beyond a critical threshold ρ_c ^{10, 28}, the actomyosin network dynamics transition from stable active non-contractile fluctuations to irreversible contractile flows. Actomyosin network contraction results in alterations to the F-actin network structure²⁷ and dynamics⁸ (Fig 2a). It has been shown previously that filament buckling coincides with network contraction as it shortens the end-to-end filament length^{29, 30}. Consistent with the change in filament curvature during buckling, the local nematic alignment is reduced during contraction (Fig 2b, Supplementary Figure 3). The question remains whether contraction is the only mechanism by which activity changes the alignment order.

Myosin is added at a fixed concentration and accumulates on the F-actin network over a couple minutes (~ 120 seconds). As myosin accumulates over time, both the mean nematic order of the F-actin network, $\langle q \rangle$, and the divergence of the F-actin velocity decreases (Fig 2b). However, loss

of order precedes the drop in divergence (Supplementary Movie 2). To disentangle time-dependent effects from myosin density accumulation, we control the onset of myosin contraction using a network saturated in blebbistatin, a pharmacological agent used to inhibit myosin ATPase activity. When illuminated with 405 nm light, blebbistatin is inactivated, reactivating myosin and allowing precise temporal control of network contraction. Using this protocol, all of the myosin has accumulated at the time of light-induced activation and the change in order and contraction occur simultaneously (Supplementary Figure 4). Thus, the loss of order depends upon myosin concentration.

In contrast to contractile networks ($\rho > \rho_c$), non-contractile networks ($\rho < \rho_c$) lose nematic order upon the addition of myosin without a significant increase in the magnitude of the divergence of the velocity field, i.e. no flow (Fig 2c). We use the maximum magnitude of the strain rate, ψ , as a measure of network contractility over the experimental timescale (~ 500 s). We vary the myosin concentration across experiments and define stable non-contractile networks as those with $|\psi| < \psi_c = 2 \times 10^{-3} \text{ s}^{-1}$. Both non-contractile networks and passive thermal networks ($\rho = 0$) exhibit ψ values over a similar range. Reorganization of the F-actin network in contractile systems leads to the loss of approximately 50% of the nematic order, in contrast to non-contractile actomyosin networks, which preserve $\geq 70\%$ of their nematic order consistently across three myosin isoforms (Fig 2d).

Myosin motor activity results in alterations of the F-actin network architecture for stable networks to the same extent for all three myosin isoforms used: skeletal muscle myosin (SkMM), non-muscle myosin (NMM), and smooth muscle myosin (SmMM) (Supplementary Figure 4). It remains unclear how the actomyosin network maintains stability in the presence of myosin-driven active stresses for non-contractile systems. Therefore, we compare the configurations of our non-

contractile active nematics to passive nematics in order to distinguish the mechanical origin of stability in active, non-contractile networks.

F-actin fluctuation correlations show length-dependent scaling behavior

Upon visual inspection, there are significant differences between the F-actin fluctuations in passive and active non-contractile systems (Fig 3 a,b). To quantify these differences, we measured the equal-time spatial autocorrelation function of the F-actin density fluctuations and the nematic director fluctuations perpendicular to the local axis of F-actin alignment (director), \hat{e}_\perp (Fig 3c, Supplementary Note). Fourier transformation of these autocorrelation functions yields the density, S_{cc} , and nematic director, S_{nn} , fluctuation spectrums for all accessible wave numbers perpendicular to the local nematic director, $|k_\perp|$ (Fig 3 c,d,e, Supplementary Figure 6). The magnitude of the fluctuation spectrum represents the fractional signal variance at the associated wavenumber³¹, while the scaling exponent signifies the physical origin of the underlying dynamic interactions in the network³ (Supplementary Table, Supplementary Figure 5).

According to active gel theory, the equal time autocorrelation of the nematic director fluctuations perpendicular to the director axis should scale as $S_{nn}(k_\perp) \sim k_\perp^{-2}$ for all k_\perp ^{32, 33}. In both passive (0.25% MC) and active non-contractile networks (0.25% MC + myosin), the F-actin director fluctuations exhibit $S_{nn}(k_\perp) \sim k_\perp^{-2}$ at large wave numbers, as predicted for equilibrium nematic liquid crystals and active gels (Fig 3e, Supplementary Figure 5)^{32, 33, 34}. This large k_\perp scaling behavior of the nematic director fluctuations originates from elastic interactions that tend to orient the filaments in the same direction³ (Fig 3 d,e). However, the director fluctuations deviate from the predicted k_\perp^{-2} scaling at small wave numbers and approach a plateau value $S_{nn}(k_\perp \rightarrow 0) \sim k_\perp^0$, indicating uncorrelated fluctuations at large wavelengths for all experimental conditions (Fig

3e, Supplementary Figure 5). In contrast, F-actin networks composed of short filaments ($l = 2.5 \pm 0.9 \mu\text{m}$), severed via gelsolin, scale as $S_{nn}(k_{\perp}) \sim k_{\perp}^{-2}$ over all accessible wavenumbers, matching theoretical predictions (Fig 3e, inset).

Active, non-contractile networks driven by SkMM exhibit the largest magnitude at small k_{\perp} , with the purely thermal (0.25% MC) and α -actinin crosslinked F-actin networks plateauing at similar values as the motor driven system. Across the myosin isoforms, the director correlation magnitude at small k_{\perp} appears to increase with the average thick filament length (SkMM > SmMM > NMM; Supplemental Figure 3). At lower concentrations of MC (0.15% MC) or in the presence of FimA2, F-actin networks exhibit lower nematic order and exhibit distinct low magnitude plateaus at small k_{\perp} . No significant differences in magnitude between the experimental conditions are observed at large k_{\perp} .

The density fluctuations orthogonal to the local nematic director are found to decay faster than the predicted k_{\perp}^{-4} scaling (Fig 3d) for density fluctuations driven by diffusion and orientation fluctuations. Similar to the director fluctuations, the transverse density fluctuations begin to plateau at small wave numbers $S_{cc}(k_{\perp} \rightarrow 0) \sim k_{\perp}^0$, signaling a loss of correlated F-actin density fluctuations over these length scales. In networks composed of short actin filaments, the density fluctuations reproduce the predicated k_{\perp}^{-4} scaling at large k_{\perp} , and exhibit a slower decay ($S_{cc} \sim k_{\perp}^{-2}$) at smaller wavenumbers (Fig 3d, inset).

The plateaus seen at small k_{\perp} for both the nematic director and density fluctuations arise from the organization of F-actin into nematic-like ordered domains that are smaller than the field of view over which the measurements are made (Fig 1c), acting as a correlation length for nematic alignment. Once we begin to probe autocorrelations beyond the average size of the nematic-like

ordered domains ($\sim 10 \mu\text{m}$), no dependence of the fluctuation correlations on length is expected. Thus, F-actin networks, composed of long, semi-flexible filaments, form nematic-like ordered viscoelastic networks that lack long-ranged order, in the presence or absence of active motor forces.

In summary, we show that myosin-driven fluctuation correlations of long F-actin exhibit a greater decay than active nematic models at short length scales. However, as the fluctuations across both passive and active samples are indistinguishable at large k_{\perp} (Supplementary Figure 6, 7), we next analyze how fluctuations differ with respect to their components parallel and perpendicular to the filament axis to quantify how myosin influences filament dynamics in non-contractile, active networks.

Non-aligned actomyosin drives F-actin bending in non-contractile, active networks

The equal-time, spatial velocity autocorrelation function, C_{vv} , of F-actin filaments decays exponentially for all non-contractile networks, both passive (0.25% MC and 0.15% MC) and active (SkMM, NMM, SmMM). The active networks decay with length scales proportional to the myosin filament length (Fig 4a, exponents in inset, filament lengths in Supplementary Figure 4). We next investigate the anisotropic velocity autocorrelation, $\delta C_{vv}(r) \equiv \langle C_{vv}^{\perp}(r) - C_{vv}^{\parallel}(r) \rangle$ to quantify the difference in the actin's motion both perpendicular and parallel to its local nematic alignment (Supplementary Note). We find that all non-contractile systems exhibit enhanced fluctuations perpendicular to the local nematic director, in stark contrast with contractile systems that show larger correlations parallel to the filament's axis (Fig 4b), as would be expected for sarcomeric contraction^{15, 35}. Even further, active non-contractile systems in particular show myosin-derived transverse fluctuations which we term “plucking” (Fig 4c, Supplementary Movie 4), in stark contrast with the canonical view of myosin activity sliding pairs of F-actin along their long axis.

Plucking may therefore be indicative of stresses that originate from non-aligned F-actin and myosin thick filaments^{10, 36}.

To investigate this possibility, we measure the relative angle between skeletal muscle myosin II (SkMM) thick filaments and the actin it decorates for a contractile network (Fig 5). SkMM is used due to its large, discernible aspect ratio. As myosin accumulates, the local concentration of myosin increases with time, allowing us to compare the difference in relative angles of actin and myosin as the network transitions from non-contractile to contractile. The relative myosin-actin angle reaches a minimum before the actomyosin network reaches the minimum value of its velocity divergence, while the density of the myosin present only marginally increases. This anisotropy in the myosin and actin alignments may therefore result in the plucking dynamics observed in non-contractile networks. The difference in length scale over which motion perpendicular and parallel to filament alignment correlate provide a marked difference between non-contractile and contractile networks, but not between active and passive systems.

Filament curvature has thus far been implicated in actomyosin contractility^{8, 26, 36, 37}, and to date, has not been associated with its stability. By examining the statistics of probe particle and filament curvature dynamics, we address the questions of activity-induced fluctuations the role of F-actin curvature in cytoskeletal stability simultaneously.

Filament plucking dissipates stress by coupling a broad spectrum of F-Actin bending modes

We measure the mean-squared displacement (MSD) of probe particle positions embedded in both active and passive actin networks. For contractile active networks, we identify a critical time, t_c , as the latest time at which the network achieves 5% of its minimum spatially averaged velocity divergence, $\langle \vec{V} \cdot \vec{v} \rangle$ (Fig 6a, blue curve). Prior to this time, the divergence of the active

network fluctuates about zero, with amplitudes larger than those of the passive network. The network is deemed non-contractile for $t < 2/3 t_c$, and contractile afterwards. The passive network never transitions to a contractile state (Fig 6a, orange curve). Probe particles embedded in the F-actin network exhibit Brownian motion, with a linearly increasing MSD for both the passive system and the active non-contractile system, with a larger magnitude in the active network (Fig 6b, solid orange and blue curves). The motion is superdiffusive (i.e. $\langle x^2 \rangle \sim t^\alpha$ with $\alpha > 1$) for the contractile system (Fig 6b, dashed blue curve). Despite the Brownian MSD, the active particles in the non-contractile network have a non-zero non-Gaussian parameter, $\alpha_2 > 0$ (Supplementary Note), a characteristic of non-equilibrium behavior³⁸, while particles in passive networks have $\alpha_2 \approx 0$ for all lag times (Fig 6c). This distinction is reflected in the broad van Hove distribution³⁹ with wide tails of particle displacements at the lag time that maximizes α_2 for the active system, consistent with previous studies⁴⁰ (Fig 6d).

The MSD of probe particles reflect bulk effects of active actomyosin networks. Inspired by the plucking motions observed in active, non-contractile networks, we assess the effect of myosin-motor activity on the individual filament bending fluctuations. To achieve this, only 1-2% of actin filaments are fluorescently labeled⁸, allowing one to track individual actin filaments within a larger network. We project the filament tracks onto the normal modes of slender rods (Supplementary Note), and track the coefficients of the mode projections in a configurational phase space. We calculate the probability currents generated in phase space^{41, 42, 43} by filament bending fluctuations (Fig 6e,f, Supplementary Figure 8, Supplementary Note), with care taken to exclude reptating filaments that may exhibit false-positive non-equilibrium fluctuations in passive networks (Supplementary Figure 9). Permuted trajectories (Supplementary Figure 10) show statistically significant circulations for a wide range of bending modes for active filaments and

zero circulation for passive filaments (Fig 6g-i), indicating mesoscopic broken detailed balance in a non-equilibrium steady state⁴⁴. While the distinct distributions for high modes could be expected as these high curvature modes are only accessed via motor activity⁸, we surprisingly see a significant difference in the distributions of low modes ($p < 0.001$, Kolmogorov-Smirnov test) which are accessible in both active and passive cases. This behavior persisted across experiments that did not eventually undergo global contraction (Supplementary Figure 9). The existence of this circulation has been predicted by recent theoretical results for exogenous probe filaments embedded in actin networks^{42, 43} and provides experimental evidence for myosin activity not acting as a temperature field while dissipating stress across all accessible length scales.

Discussion

Here, we present a novel polymeric, active nematic material whose behavior is not captured by current active nematic liquid crystal theory. We show that the interactions between filaments and molecular motors that stabilize the *in vitro* model cell cytoskeleton are not only diverse and dynamic, but also distinct from those associated with contractile flow. Despite enhanced fluctuations in velocity and elevated particle diffusivity (Fig 6a,b), there is no net material flow or contractility — our main indication of network stability — and stresses are instead dissipated by bending motion of filaments.

In this stable state we measure the magnitude and scaling behaviors of spatial fluctuations in both the nematic director and F-actin density. The nematic director fluctuations scale as k_{\perp}^{-2} for large k_{\perp} which can be explained by purely orientational elastic interactions between adjacent F-actin (Supplementary Table), followed by a plateau region that scales as k_{\perp}^0 for small k_{\perp} . The density fluctuations decay faster than k_{\perp}^{-4} at large values of k_{\perp} but again as k_{\perp}^0 at small values of

k_{\perp} . This leveling off of both the director and density fluctuations is not due to filament turnover as in previous works³, but rather to the finite size of the nematically ordered domains in the experiment. Long range interactions are lost due to the dissipation of entropic entanglements between filaments beyond a length scale set by the size of our nematic domains, beyond which spatial correlations weaken considerably. The spatial autocorrelation functions do not completely flatten out as when all memory is erased from the system by filament disassembly. In summary, we find deviations from traditional nematic liquid crystal theory that suggest that our material cannot be described using existing theory.

Enhanced transverse fluctuation of F-actin provides the clearest distinction between stable and contractile systems. Analysis of individual filament phase spaces (Fig 6) indicates that myosin activity couples orthogonal bending eigenmodes, breaking detailed balance in a way that clearly distinguishes myosin activity from a temperature which could not produce such cross-correlations. Further, these couplings exist across all bending modes analyzed, even thermally accessible modes with low curvature, indicating that stable actomyosin networks dissipate stress across all length scales available. In addition, circulations in phase space is an indication of entropy production⁴⁵. These results implicate F-actin curvature in network stability, when it has previously only been associated with contractility⁸. Thus, activity can have a hitherto unrealized stabilizing effect on engineered materials.

Finally, while we find that axial motions of F-actin, consistent with the canonical “sliding” of F-actin in muscle, are associated with contractility, stable fluctuations are surprisingly dominated by transverse filament deformations (Supplementary Movie 4), regardless of myosin isoform. These reversible F-actin plucking events are associated with transient interactions between non-aligned myosin and F-actin (Fig 5), and the bending energy of the filaments

(Supplementary Note) indicates that only a few heads are engaged to induce this reversible bending. Thus, this work challenges the prevailing model of molecular motors as idealized force dipoles in both contractile and non-contractile systems, although the specifics of myosin multivalency, binding kinetics, and size of myosin thick filaments do not seem to make a difference as all isoforms exhibit similar behaviors in contractile or non-contractile systems.

Conclusion

Dynamic stability in active nematics has thus far been associated with fluidity – the continuous sliding of rigid filaments past each other while maintaining the overall architecture and organization. However, in our system, the elasticity of F-actin is excited by non-canonical actomyosin interactions, coupling a wide spectrum of bending modes and providing new mechanistic insight into the stabilization of soft, active materials. This identification and characterization of active and elastic nematics presents a new and comprehensive understanding for mechanical and dynamic stability in active biological materials.

Acknowledgements

We thank Enrique de la Cruz for help with reagents and supplies. IAL acknowledges support from NSF Fellowship grant # GE-1256259. DSS acknowledges support from NSF Fellowship grant # DGE1122492. We acknowledge funding CMMI-1525316, ARO MURI W911NF-14-1-0403 and NIH U54 CA209992 to MM. SB acknowledges Strategic Fellowship support from the University College London. Any opinion, findings, and conclusions or recommendations expressed in this material are those of the authors(s) and do not necessarily reflect the views of the National Science Foundation.

Author Contributions

MPM and SB designed and conceived the research. MPM, IL, DSS, AT, APT, and SB acquired experimental data and performed analysis. MPM, AT, DSS, SB, PO, and IL contributed analytical methods for experimental data. MPM, DSS, IL, SB, and APT wrote the paper.

Competing Financial Interests

The authors declare no competing financial interests.

References

1. Bretschneider T, Diez S, Anderson K, Heuser J, Clarke M, Muller-Taubenberger A, *et al.* Dynamic actin patterns and Arp2/3 assembly at the substrate-attached surface of motile cells. *Current Biology* 2004, **14**(1): 1-10.
2. Banerjee S, Utuje KJ, Marchetti MC. Propagating Stress Waves During Epithelial Expansion. *Phys Rev Lett* 2015, **114**(22): 228101.
3. Bruges J, Needleman D. Physical basis of spindle self-organization. *Proceedings of the National Academy of Sciences of the United States of America* 2014, **111**(52): 18496-18500.
4. DeCamp SJ, Redner GS, Baskaran A, Hagan MF, Dogic Z. Orientational order of motile defects in active nematics. *Nature materials* 2015, **14**(11): 1110-1115.
5. Sanchez T, Chen DT, DeCamp SJ, Heymann M, Dogic Z. Spontaneous motion in hierarchically assembled active matter. *Nature* 2012, **491**(7424): 431-434.
6. Kohler S, Schaller V, Bausch AR. Structure formation in active networks. *Nature materials* 2011, **10**(6): 462-468.
7. Ronceray P, Broedersz CP, Lenz M. Fiber networks amplify active stress. *Proceedings of the National Academy of Sciences of the United States of America* 2016, **113**(11): 2827-2832.
8. Murrell MP, Gardel ML. F-actin buckling coordinates contractility and severing in a biomimetic actomyosin cortex. *Proceedings of the National Academy of Sciences of the United States of America* 2012, **109**(51): 20820-20825.
9. Silva MS, Depken M, Stuhmann B, Korsten M, Mackintosh FC, Koenderink GH. Active multistage coarsening of actin networks driven by myosin motors. *Proceedings of the National Academy of Sciences of the United States of America* 2011, **108**(23): 9408-9413.

10. Murrell M, Gardel ML. Actomyosin Sliding is Attenuated in Contractile Biomimetic Cortices. *Molecular biology of the cell* 2014.
11. Vogel SK, Petrasek Z, Heinemann F, Schwille P. Myosin motors fragment and compact membrane-bound actin filaments. *Elife* 2013, **2**.
12. Humphrey D, Duggan C, Saha D, Smith D, Kas J. Active fluidization of polymer networks through molecular motors. *Nature* 2002, **416**(6879): 413-416.
13. Chaikin PM, Lubensky TC. *Principles of condensed matter physics*. Cambridge University Press: Cambridge ; New York, NY, USA, 1995.
14. Dogic Z, Sharma P, Zakhary MJ. Hypercomplex Liquid Crystals. *Annu Rev Conden Ma P* 2014, **5**: 137-157.
15. Huxley AF. Muscle structure and theories of contraction. *Prog Biophys Biophys Chem* 1957, **7**: 255-318.
16. Huxley HE. The double array of filaments in cross-striated muscle. *J Biophys Biochem Cytol* 1957, **3**(5): 631-648.
17. Huxley HE. The Mechanism of Muscular Contraction. *Science* 1969, **164**(3886): 1356-1366.
18. Gardel ML, Nakamura F, Hartwig JH, Crocker JC, Stossel TP, Weitz DA. Prestressed F-actin networks cross-linked by hinged filamins replicate mechanical properties of cells. *Proceedings of the National Academy of Sciences of the United States of America* 2006, **103**(6): 1762-1767.
19. Viamontes J, Oakes PW, Tang JX. Isotropic to nematic liquid crystalline phase transition of F-actin varies from continuous to first order. *Phys Rev Lett* 2006, **97**(11).
20. Isambert H, Venier P, Maggs AC, Fattoum A, Kassab R, Pantaloni D, *et al*. Flexibility of Actin-Filaments Derived from Thermal Fluctuations - Effect of Bound Nucleotide, Phalloidin, and Muscle Regulatory Proteins. *Journal of Biological Chemistry* 1995, **270**(19): 11437-11444.
21. Weirich KL, Banerjee S, Dasbiswas K, Witten TA, Vaikuntanathan S, Gardel ML. Liquid behavior of cross-linked actin bundles. *Proceedings of the National Academy of Sciences of the United States of America* 2017, **114**(9): 2131-2136.

22. Koenderink GH, Dogic Z, Nakamura F, Bendix PM, MacKintosh FC, Hartwig JH, *et al.* An active biopolymer network controlled by molecular motors. *Proceedings of the National Academy of Sciences of the United States of America* 2009, **106**(36): 15192-15197.
23. Kohler S, Bausch AR. Contraction mechanisms in composite active actin networks. *PloS one* 2012, **7**(7): e39869.
24. Kohler S, Schaller V, Bausch AR. Collective dynamics of active cytoskeletal networks. *PloS one* 2011, **6**(8): e23798.
25. Schuppler M, Keber FC, Kroger M, Bausch AR. Boundaries steer the contraction of active gels. *Nature communications* 2016, **7**.
26. Ennomani H, Letort G, Guerin C, Martiel JL, Cao W, Nedelec F, *et al.* Architecture and Connectivity Govern Actin Network Contractility. *Current biology : CB* 2016, **26**(5): 616-626.
27. Soares e Silva M, Depken M, Stuhmann B, Korsten M, MacKintosh FC, Koenderink GH. Active multistage coarsening of actin networks driven by myosin motors. *Proceedings of the National Academy of Sciences of the United States of America* 2011, **108**(23): 9408-9413.
28. Linsmeier I, Banerjee S, Oakes PW, Jung W, Kim T, Murrell MP. Disordered actomyosin networks are sufficient to produce cooperative and telescopic contractility. *Nature communications* 2016, **7**: 12615.
29. Lenz M, Gardel ML, Dinner AR. Requirements for contractility in disordered cytoskeletal bundles. *New J Phys* 2012, **14**(3): 033037.
30. Lenz M, Thoresen T, Gardel ML, Dinner AR. Contractile units in disordered actomyosin bundles arise from F-actin buckling. *Phys Rev Lett* 2012, **108**(23): 238107.
31. Howard J. *Mechanics of Motor Proteins and the Cytoskeleton*. Sinauer Associates: Sunderland, Massachusetts, 2001.
32. Marchetti MC, Joanny JF, Ramaswamy S, Liverpool TB, Prost J, Rao M, *et al.* Hydrodynamics of soft active matter. *Rev Mod Phys* 2013, **85**(3).
33. Kruse K, Joanny JF, Julicher F, Prost J, Sekimoto K. Generic theory of active polar gels: a paradigm for cytoskeletal dynamics. *Eur Phys J E* 2005, **16**(1): 5-16.
34. Gennes PGd. *The physics of liquid crystals, by p. G. de Gennes*. Clarendon Press: Oxford [Eng.], 1974.

35. Huxley AF, Niedergerke R. Structural changes in muscle during contraction; interference microscopy of living muscle fibres. *Nature* 1954, **173**(4412): 971-973.
36. Lenz M. Geometrical Origins of Contractility in Disordered Actomyosin Networks. *Phys Rev X* 2014, **4**(4).
37. Paluch E, Piel M, Prost J, Bornens M, Sykes C. Cortical actomyosin breakage triggers shape oscillations in cells and cell fragments. *Biophysical journal* 2005, **89**(1): 724-733.
38. Rahman A. Correlations in Motion of Atoms in Liquid Argon. *Phys Rev* 1964, **136**(2a): A405-+.
39. Weeks ER, Crocker JC, Levitt AC, Schofield A, Weitz DA. Three-dimensional direct imaging of structural relaxation near the colloidal glass transition. *Science* 2000, **287**(5453): 627-631.
40. Toyota T, Head DA, Schmidt CF, Mizuno D. Non-Gaussian athermal fluctuations in active gels. *Soft matter* 2011, **7**(7): 3234-3239.
41. Battle C, Broedersz CP, Fakhri N, Geyer VF, Howard J, Schmidt CF, *et al.* Broken detailed balance at mesoscopic scales in active biological systems. *Science* 2016, **352**(6285): 604-607.
42. Gladrow J, Broedersz CP, Schmidt CF. Nonequilibrium dynamics of probe filaments in actin-myosin networks. *Phys Rev E* 2017, **96**(2).
43. Gladrow J, Fakhri N, MacKintosh FC, Schmidt CF, Broedersz CP. Broken Detailed Balance of Filament Dynamics in Active Networks. *Phys Rev Lett* 2016, **116**(24).
44. Zia RKP, Schmittmann B. Probability currents as principal characteristics in the statistical mechanics of non-equilibrium steady states. *J Stat Mech-Theory E* 2007.
45. Lan G, Sartori P, Neumann S, Sourjik V, Tu YH. The energy-speed-accuracy trade-off in sensory adaptation. *Nature Physics* 2012, **8**(5): 422-428.
46. Murrell M, Thoresen T, Gardel M. Reconstitution of contractile actomyosin arrays. *Methods in enzymology* 2014, **540**: 265-282.
47. Kovacs M, Toth J, Hetenyi C, Malnasi-Csizmadia A, Sellers JR. Mechanism of blebbistatin inhibition of myosin II. *The Journal of biological chemistry* 2004, **279**(34): 35557-35563.

48. Limouze J, Straight AF, Mitchison T, Sellers JR. Specificity of blebbistatin, an inhibitor of myosin II. *Journal of muscle research and cell motility* 2004, **25**(4-5): 337-341.
49. Cetera M, Ramirez-San Juan GR, Oakes PW, Lewellyn L, Fairchild MJ, Tanentzapf G, *et al.* Epithelial rotation promotes the global alignment of contractile actin bundles during *Drosophila* egg chamber elongation. *Nature communications* 2014, **5**: 5511.
50. Smith MB, Li H, Shen T, Huang X, Yusuf E, Vavylonis D. Segmentation and tracking of cytoskeletal filaments using open active contours. *Cytoskeleton* 2010, **67**(11): 693-705.
51. Aragon SR, Pecora R. Dynamics of Wormlike Chains. *Macromolecules* 1985, **18**(10): 1868-1875.

Methods

Assay construction

Assay Construction is performed as described previously⁴⁶. Briefly, a phospholipid bilayer composed of 99.8% Egg Phosphatidyl-Choline (EPC, Avanti Polar Lipids) and 0.2% Oregon Green 1,2-Dihexadecanoyl-sn-Glycero-3-Phosphoethanolamine (OG-DOPC, Molecular Probes) is deposited onto a UV-treated or Piranha-treated coverslip. Stabilized F-actin (1 μM) with 0.3 μM fluorescent actin (Alexa-Fluor 568, Molecular Probes) is sedimented to the surface of the bilayer using 0.25% methyl-cellulose (Sigma). Skeletal-muscle myosin (10.5 μM stock), smooth-muscle myosin and non-muscle myosin II monomers (2.4 μM stock) are then added to the F-actin network. As the actual concentration within a microscopic field of view can vary, the precise concentration of myosin is calculated by visualizing the labelled myosin in experiment, and calculating the density of myosin thick filaments per unit area ($\#/\mu\text{m}^2$) from the fluorescence images^{28, 47, 48}.

Myosin isoforms

Smooth muscle and non-muscle isoforms are purified, polymerized and fluorescently labelled according to standard protocols⁴⁶. Skeletal muscle myosin (Cytoskeleton) and other isoforms are stained using Alexa-647 (Molecular Probes). Skeletal muscle myosin is used to assess alignment between thick and thin filaments due to its length (~2 μm). Smooth muscle myosin is used to assess F-actin deformation due to slower motor kinetics. Skeletal and non-muscle isoforms are also used for light activation as they are sensitive to blebbistatin ATPase inactivation.

Confocal microscopy is used to image the dynamics of fluorescent protein with the assay. Images are recorded on a Zyla 4.2 Megapixel sCMOS camera on a Leica microscope and also recorded on a Coolsnap Hq2 CCD Camera on a Nikon Ti Inverted Microscope.

F-actin alignment, fluctuations, and correlations are calculated using custom Matlab written routines (see Supplementary Note).

Nematic order parameter calculations

The nematic order parameter, q , is calculated using custom Matlab code. A custom MATLAB algorithm is used to extract the F-actin director field from images of fluorescently labeled F-actin, as described previously⁴⁹. Briefly, fluorescent images are divided into small, overlapping 3.5 μm by 3.5 μm windows, and the local F-actin orientation (director) is calculated for each window, yielding an F-actin director field over an image. To determine the local F-actin director, each window is Gaussian filtered and transformed into Fourier space using a 2D fast Fourier Transform (FFT). The axis of the least second moment was calculated from the second order central moments of the transformed window, and the angle of the local F-actin director is defined as orthogonal to this axis. Next, the local degree of alignment is calculated between

adjacent windows within 3x3 kernels. The local nematic order is calculated for the central window in each kernel using the modified order parameter equation $q = 2 \cdot \langle \cos^2(\theta) - \frac{1}{2} \rangle$, where θ is the difference in F-actin orientation between the central window and the 8 surrounding windows. This process is repeated for all possible 3x3 kernels over an image, yielding a nematic director field with defined director magnitude and orientation for each window over an image. Perfect alignment between adjacent regions within an F-actin network results in an order parameter equal to one. Conversely, orientation differences of 45 degrees (maximum expected for quasi-2D F-actin network) between adjacent regions of the network result in an order parameter equal to zero.

Flow calculations

Particle image velocimetry (PIV) is applied in Matlab (mPIV, <https://www.mn.uio.no/math/english/people/aca/jks/matpiv/>) to fluorescent F-actin images, yielding displacement & velocity vector fields.

Fluctuation correlations

Using custom Matlab code, the local alignment field, nematic order parameter, and density scalar field are extracted for each confocal image. The equal time autocorrelation function for both the nematic director and the density fields are calculated at every position in the image along an axis transverse to the local alignment field, and the results are binned across all time and space for each experimental condition. See Supplementary Note for more details

Particle tracking

The MSD is calculated for actomyosin networks with ~1 μ m beads embedded throughout the network. The beads are tracked both before (passive) and after (active) NMM is added to the network. MSDs are calculated using software freely available from the Kilfoil lab

[<http://people.umass.edu/kilfoil/downloads.html>]. All systems are imaged over 200-300 s, leading to MSDs that are measureable for just over 100 s each.

Probability flux loop analysis

Individual actin filaments are tracked using the ImageJ plugin JFilament⁵⁰ over time. Their motion is decomposed into the eigenmodes of the Langevin equation for the transverse displacements, $u(s,t)$, of the filament as a function of arc length, s , and time, t ⁵¹. The coefficients of the eigenmodes are calculated over time and used to construct the phase space trajectory of each filament. The phase space is discretized and cumulative fluxes are calculated. The curl of the flux field measures the net circulation, and the statistical significance of the curl is found via a permutation method. Reptating filaments were excluded from the analysis due to the possibility of false-positive results (Supplementary Figure 9) and robustness of the measured curls was assessed by a permutation test on the original trajectory (Supplementary Figure 10). See Supplementary Note for more details.

Figures

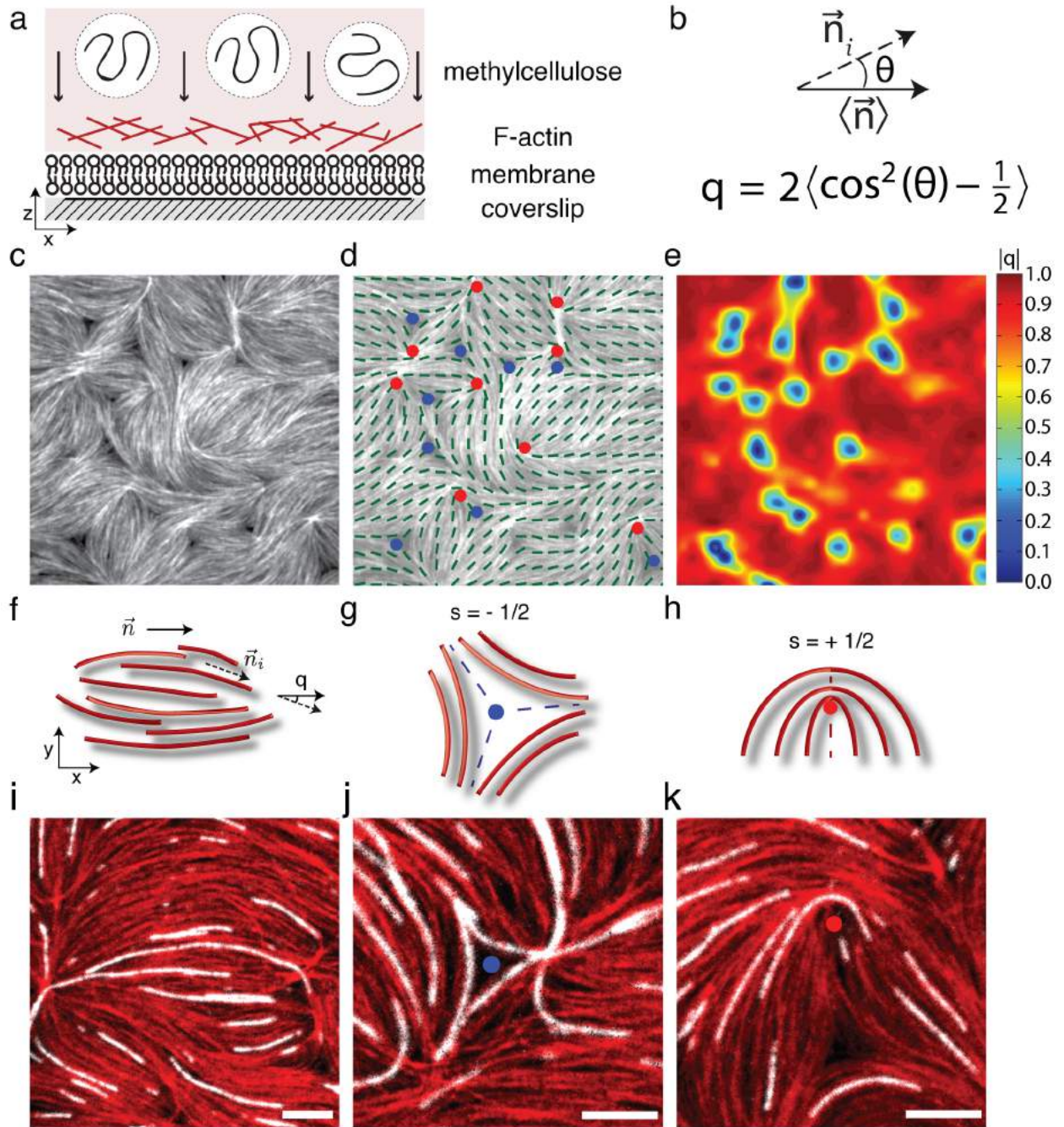


Figure 1. Synthesis of a soft nematic using a biomimetic actomyosin cortex.

(a) Schematic of stabilized F-actin sedimentation onto a phospholipid bilayer by depletion agents proximal to a hydroxylated coverslip. (b) Functional form of 2D nematic order parameter used to

calculate the degree of alignment in F-actin networks. (c) Fluorescent F-actin crowded to the bilayer. Scale bar represents 10 μm . (d) Location of disclinations with topological charges $s=-1/2$ and $s=+1/2$, shown by blue and red dots respectively. Green lines represent nematic director of the F-actin gel. (e) Magnitude of the nematic order parameter (q) which shows hot colors where the nematic order is high, and cool colors where the alignment is low. (f) Schematic of a nematically ordered domain comprised of many F-actin filaments, where \vec{n} is the nematic director of the entire domain, \vec{n}_i is the local alignment of a single F-actin, and θ is the angle between them. (i) Image of a single nematic domain. Both red and white actin filaments, labeled with different fluorophores and polymerized separately, are combined at a large ratio prior to crowding to show individual filaments within the larger network. (g) Schematic and (j) data of a $-1/2$ disclination defect and local nematic ordering in quasi 2D F-actin¹³. (h) Schematic and (k) data of a $+1/2$ disclination defect and local nematic ordering in quasi 2D F-actin network. Scale bars (i-k) represent 5 μm .

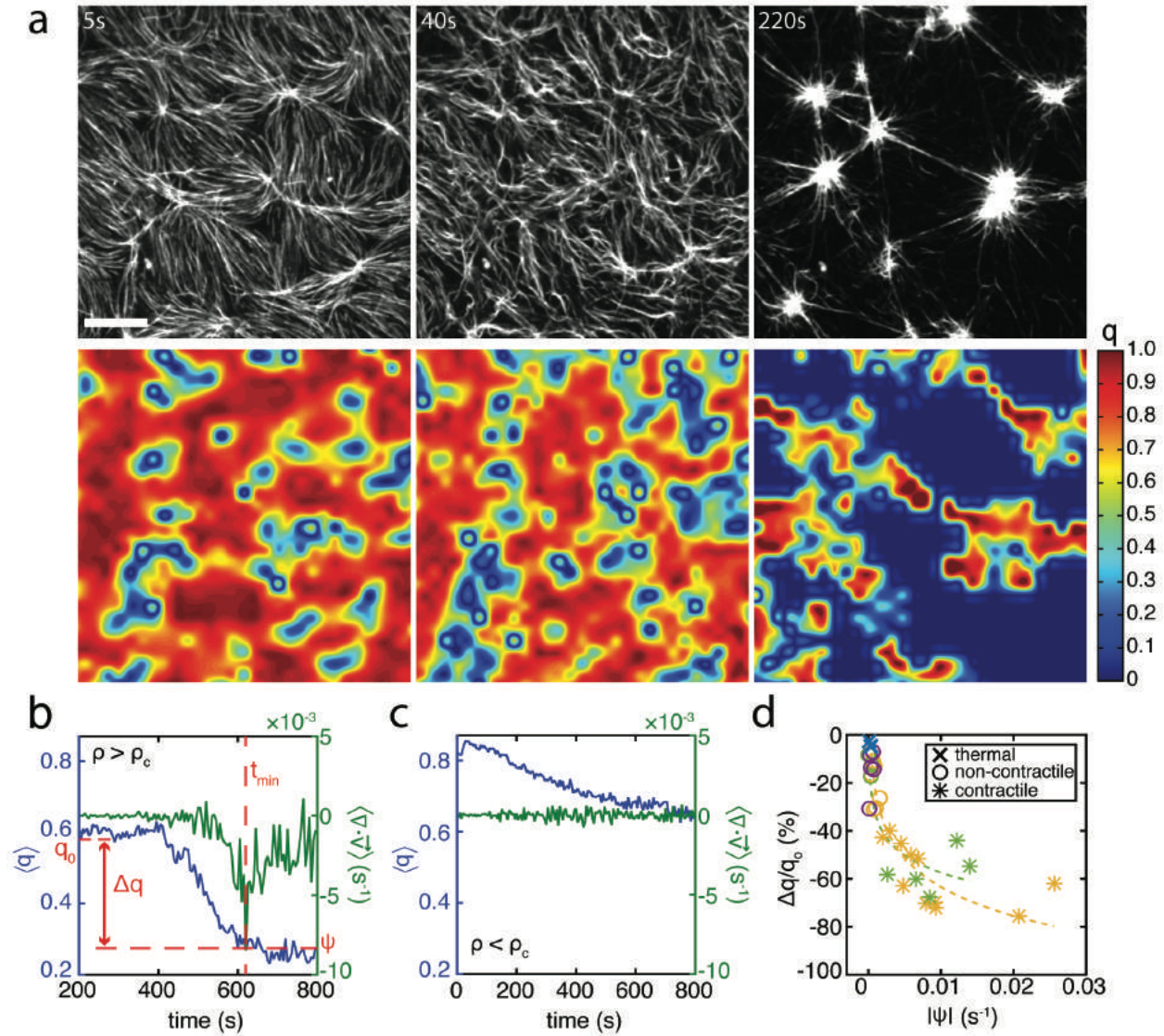


Figure 2. F-actin nematic order is altered by myosin density in both contractile and non-contractile states.

(a) Top: F-actin network undergoing contraction. Bottom: magnitude of nematic order parameter q during F-actin contraction. Hot colors indicate high alignment, and cool colors indicate low alignment. Scale bar represents 10 μm . (b) Spatially averaged F-actin nematic order parameter (blue) and mean divergence of F-actin velocity (green) 200s after the onset of myosin addition ($\rho > \rho_c$). Time of minimum divergence (ψ) indicated by vertical dotted red line. Difference

between nematic order at $t=0$ and at time of minimum divergence ($\Delta q = q(0) - q(t_{\min})$) indicated by horizontal dotted red line. (c) Spatially averaged nematic order (blue) and divergence of the velocity (green) for a non-contractile actomyosin network ($\rho < \rho_c$), where myosin is added at $t=0$. (d) Change in nematic order ($\Delta q/q_0$) for thermal (\times), non-contractile (\circ), and contractile ($*$) network states. The marker color denotes the myosin isoform added to each experiment (SkMM= yellow, SmMM = green, NMM = purple, no myosin = blue).

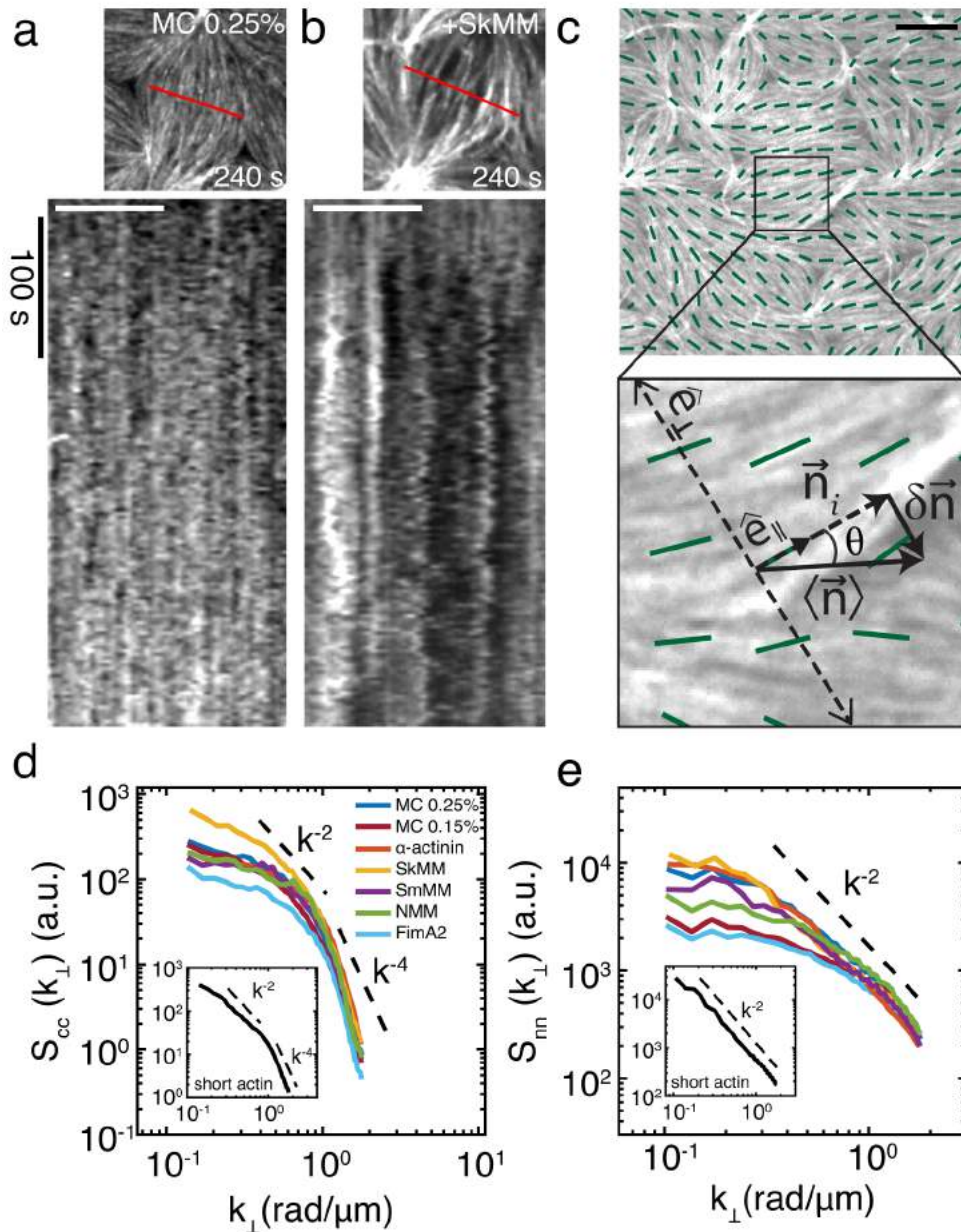


Figure 3. F-actin fluctuations deviate from active gel theory for networks composed of long actin filaments

(a,b) Kymograph across a single nematic domain of a 2D F-actin network in the presence of 0.25% methyl cellulose (MC) alone (a), and 0.25% MC + skeletal muscle myosin (SkMM, b). White scale bar is 5 μm (c) 2D F-actin network in the presence of 0.25% MC with alignment vector field (green), scaled by the local nematic order parameter, overlaid. Lower panel shows a schematic of the local alignment vector (\vec{n}_i), local coordinate system defined by the axes parallel (\hat{e}_{\parallel}) and perpendicular (\hat{e}_{\perp}) to the local alignment vector, and local alignment vector fluctuations ($\delta\vec{n}_i \equiv \vec{n}_i - \langle \vec{n}_i \rangle$) used to calculate fluctuation correlations. Scale bar represents 10 μm (d,e) Equal time spatial density-density (S_{cc}) and director-director (S_{nn}), fluctuation autocorrelations, respectively, along the local perpendicular axis (c, lower) as a function of the perpendicular wave vector (k_{\perp}). The spatial autocorrelations are shown for different experimental conditions within the *in vitro* F-actin cortex model, where each condition is an average of several experiments: 0.25% MC (N = 16), 0.15% MC (N = 8), α -actinin (1:30 α -actinin:actin, N = 5), skeletal muscle myosin (SkMM, N = 6), smooth muscle myosin (SmMM, N = 4), non-muscle myosin (NMM, N = 3), FimA2 (10 nM, N = 5), and short actin filaments (insets), $\langle l \rangle = 2.5 \pm 0.9 \mu\text{m}$ ($N_{\text{fils}} = 200$). All experiments contain the same concentration of F-actin (1.32 μM) with 0.25% MC, unless specified otherwise. The dashed black lines (d,e) follow the predicted correlation decay by active nematic liquid crystal theory: k_{\perp}^{-2} for S_{nn} (e) and either k_{\perp}^{-2} or k_{\perp}^{-4} for S_{cc} (d), depending on the system composition and the length scale of interest.

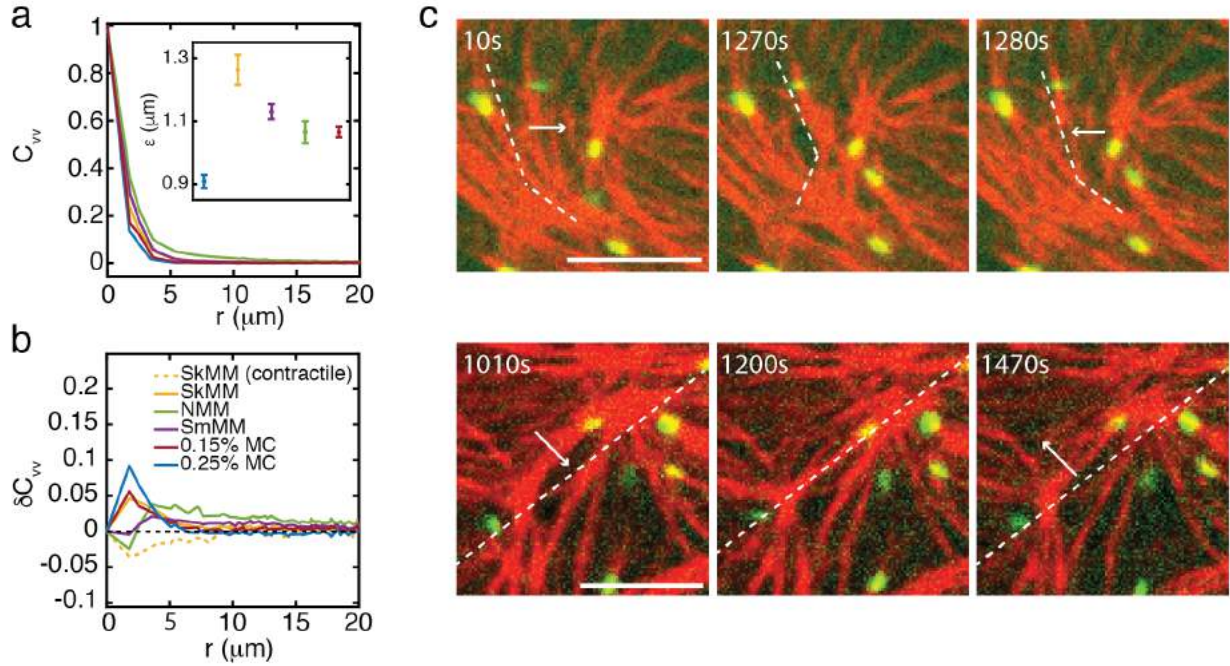


Figure 4. Individual transverse F-actin fluctuations dominate non-contractile actomyosin.

(a) Velocity autocorrelation function of non-contractile F-actin as a function of separation distance, r , exhibiting a stretched exponential decay with correlation length specified in the inset (mean \pm std). Averages are taken across several experiments ($N_{\text{SkMM}} = N_{0.25\% \text{MC}} = N_{0.15\% \text{MC}} = 3$, $N_{\text{SmMM}} = 5$, $N_{\text{NMM}} = 2$), where each experiment is represented by its own temporal average. The colors represent different experimental conditions given by the legend in (b). (b) Anisotropic velocity-velocity, $\delta C_{vv}(r) \equiv \langle C_{vv}^{\perp}(r) - C_{vv}^{\parallel}(r) \rangle$. (c) Myosin driven motions of F-actin perpendicular to the filament axis within an actomyosin network. Images of 40 nM smooth muscle myosin (green) embedded within $\sim 1\mu\text{M}$ F-actin network (red). White dotted lines indicate alignment of F-actin. White arrows indicate direction of motion of F-actin. Scale bars represent 5 μm .

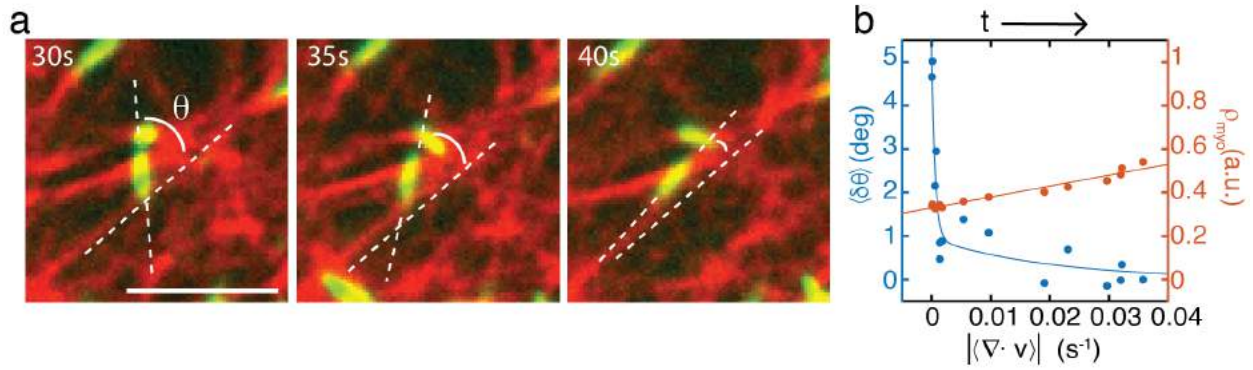


Figure 5: Myosin is misaligned with underlying actin for non-contractile networks.

(a) Images of $\sim 1 \mu\text{M}$ actin and 40 nM skeletal muscle myosin. Angle θ is measured between the myosin thick filament and the F-actin it sits upon. Scale bar is $5 \mu\text{m}$. (b) Average change in angle ($\langle \delta\theta(t) \rangle = \langle \theta(t) - \theta(\infty) \rangle$) of myosin thick filaments (blue dots) and normalized mean fluorescent intensity of myosin (orange dots) as functions of the average divergence of the velocity field of the F-actin, which increases from 0 to 0.04 s^{-1} as time increases. Solid lines are guides for the eye.

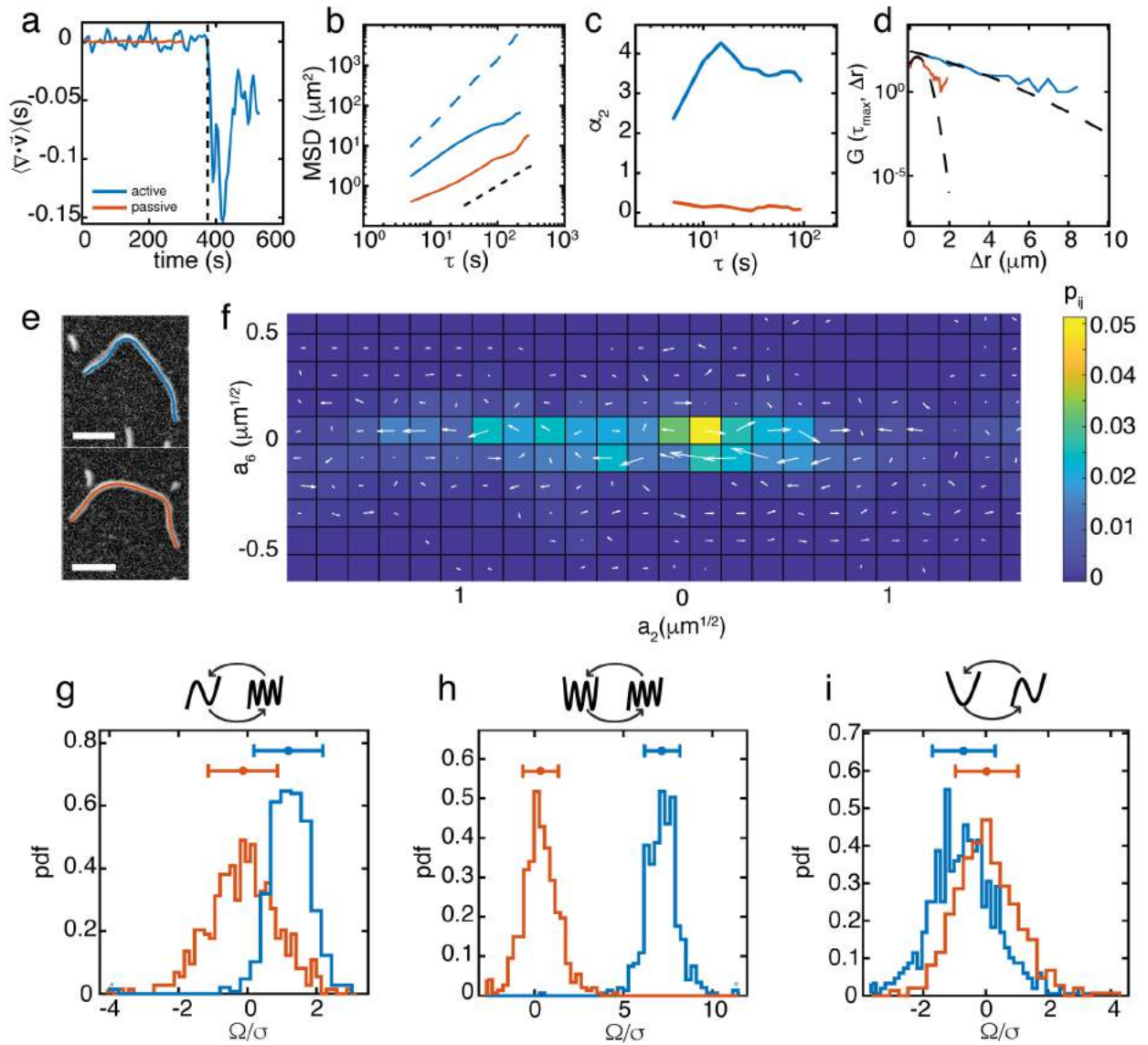


Figure 6: Non-contractile actomyosin networks couple filament bending modes in a non-equilibrium steady state.

(a) The mean divergence of the actin in the experiment tracked using PIV, establishing t_c as the last time the divergence reaches 5% of its minimum value. Blue and orange lines are active and passive experiments. t indicates time from the addition of myosin thick filaments (blue) and arbitrary time after F-actin sedimentation (orange). (b) The MSD of tracked beads in an active

experiment at times $t > 2/3 t_c$ (dotted blue line), $t < 2/3 t_c$ (solid blue line), and a passive experiment (solid orange line). Black dotted line has slope=1. (c) First non-Gaussian parameter in 2-dimensions for active and passive experiments. (d) Van Hove function for the lag time that maximizes the non-Gaussian parameter for active and passive experiments. Black dotted line is a Gaussian fit to each distribution. (e) Image of a typical actin filament before myosin is added (bottom), and after (top). Scale bar is 5 μm . (f) Subsection of the coarse-grained phase space for $n=18$ active filaments using the time series of hydrodynamic mode coefficients for modes 2 and 6. Color indicates the fraction of total experiment time spent within each state in the phase space. (g-i) Histogram of circulation normalized by the standard deviation of the histogram for $N=500$ bootstrapped trajectories for subspaces spanned by modes 2 and 6 (g), 5 and 6 (h), and 1 and 2 (i). Blue and orange indicate active and passive experiments as above. Dots and bars indicate means and standard deviations of each normalized distribution.